Tribology International 130 (2019) 334–338

Contents lists available at ScienceDirect

Tribology International

journal homepage: www.elsevier.com/locate/triboint

Supporting and friction properties of magnetic fluids bearings

Zhengdong Hu, Zhuang Wang, Wei Huang*, Xiaolei Wang

College of Mechanical & Electrical Engineering, Nanjing University of Aeronautics & Astronautics, Nanjing, 210016, China

ARTICLE INFO

Keywords:
Magnetic fluids
Magnetic field strength
Load carrying capacity
Lubrication

ABSTRACT

A driblet of magnetic fluids (MFs) falls on an annular magnet, forming a closed liquid ring. The magnetized MFs can produce liquid support due to magnetostatic force. The air cushion enclosed by the MFs sealing ring may generate gas support as the magnet bottom combines with a substrate. The supporting capacity supplied by the liquid-gas contributes to friction reduction. Research shows such supporting is affected by the surface magnetic field and field distribution. Tribological results confirm that low friction can be obtained since the tribo-pairs are separated by the supporting force and the friction originates from the fluid viscosity. Such design would be significant for solving the “cold welding” as well as the “stick-slip” phenomenon, especially in precise sliding machine.

1. Introduction

Magnetic fluids (MFs) are colloidal suspensions, which contain single domain ferromagnetic nanoparticles dispersing in a carrier liquid [1]. Brownian movement maintains these particles from sinking under gravity effect and a suitable organic surfactant is coated around each particle to overcome agglomeration due to van der Waals force and magnetic dipole interaction [2]. The behaviors of MFs mainly depend on their magnetic properties and the fluids may automatically flow and stay into regions with more intense magnetic field. This feature of magnetic controlling has attracted many scientific and industrial applications, such as rotary shaft sealing [3], grinding [4] and separation [5].

Lubrication is also a typical application of MFs [6]. Compared with traditional liquid lubricants, the superiority of MFs as lubricant is that it can be attracted in the contact zone by an external magnetic field and still possess fluidity at the same time [7]. From the lubrication point of view, this enables the supply of lubricant for the friction pairs without the use of pumps. Further more, the magnetization of the MFs interacts with the applied magnetic field to generate attractive forces on the particles. Due to the stabilized suspension of magnetic particles in the fluid, the attractive magnetic force manifests itself as a body force on the fluid [8]. Therefore, the local concentrated MFs under magnetic field can generate a controllable body force or magnetostatic force acting as a buoyancy force to separate the tribo-pairs [9,10].

Besides the magnetostatic supporting of the liquid, MFs seal may produce a kind of gas supporting [11,12], which is also beneficial for lubrication. As shown in Fig.1a, a drop of MFs was absorbed on the surface of an annular magnet, forming an enclosed liquid structure. When the bottom of the magnet is open, the magnetized MFs structure provides magnetostatic force only. While a substrate is combined with the magnet bottom without leakage, beside the magnetostatic force, the air in the chamber packaged by the MFs seal might also produce gas supporting force. Thus, the load carrying capacity will be shared by the magnetized liquid and the sealed gas together (see Fig. 1b).

Compared with magnetostatic force, the participation of the gas support will further enhance the load carrying capacity. When the gross weight of object is less than the bearing force, it may be totally held and floated up. For precise machinery, direct contact between friction surfaces can be avoided and full fluid film can be achieved. Different from hydrodynamic lubrication, the main superiority of such structure is that the load carrying capacity does not rely on the relative motion of two surfaces. Moreover, it still exists between two parallel planes. Therefore, compared with traditional fluid lubrication, the novelty of such supporting construction is that, ultralow friction can be expected even at low or relatively static state and the “stick-slip” phenomenon may be avoided, which is highly desirable in friction system.

In the previous refs. [11,12], attention was paid on the principle analysis of such supporting system and few experiments were carried out. Meanwhile, the contribution of the magnetostatic force was neglected. And in the supporting process, which one serves as the main role, the liquid or gas? Besides, are there any effective methods for upgrading the supporting force? Furthermore, can ultralow friction be achieved based on this supporting system? There is little knowledge about it.

In this paper, the load carrying capacity of the supporting

* Corresponding author. Yudao street 29#, Nanjing, China.
E-mail address: huangwei@nuaa.edu.cn (W. Huang).

https://doi.org/10.1016/j.triboint.2018.10.006
Received 23 August 2018; Accepted 7 October 2018
Available online 09 October 2018
0301-679X/ © 2018 Elsevier Ltd. All rights reserved.

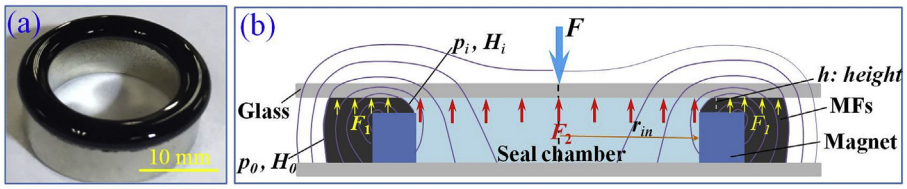

Fig. 1. (a) The image of an annular magnet covered with MFs, (b) Supporting schematic diagram.

construction was analyzed considering the magnetostatic force. The gas supporting force was obtained indirectly via experiments and the value was compared with theoretical results. After that, two simple ways were proposed to further enhance the supporting force: 1) increasing the surface magnetic property of magnet; 2) changing magnet distribution. Finally, the lubrication behaviors of such system were evaluated.

2. Theory analysis

The principle diagram of the supporting system was shown in Fig. 1b. When ignoring the weight of the upper glass, the expression, according to the force equilibrium condition, can be written as:

$$F + p_0 A_F = F_1 + p_i A_F \tag{1}$$

where F is the normal load, p_0 (bar pressure) and p_i are the hydrostatic pressures on the two sides of the MFs interface and A_F is the supporting surface area. F_1 is the magnetostatic force of magnetized MFs, which can be measured directly (see in the results section). Then, the total supporting force may be presented by:

$$F = F_1 + (p_i - p_0)A_F \tag{2}$$

here, $(p_i - p_0)$ is the pressure difference across the MFs interface. As can be seen, the load F can be written in a form of liquid-gas mixed support:

$$F = F_1 + F_2 \tag{3}$$

where F_1 is the magnetostatic force of magnetized liquid, F_2 is the force generated by the gas pressure difference across the MFs interfaces.

When ignoring the surface tension and gravity of MFs, according to MFs sealing principle, the pressure difference applied to the MFs is expressed by Ref. [13]:

$$p_i - p_0 = \mu_0 \int_{H_0}^{H_i} M \, dH = \mu_0 M (H_i - H_0) \tag{4}$$

where M is the magnetization of MFs, H_i and H_0 are the corresponding magnetic intensity on each side of the MFs interface. Usually, for a N35 NdFeB magnet, the magnetic field in the sealing gap (within 1 mm) reaches 10^5 A/m and MFs can be regarded as fully saturated (M_s) [8]. Thus, F_2 can be written as:

$$F_2 = \mu_0 M_s (H_i - H_0) A_F \tag{5}$$

where A_F is the gas supporting area ($A_F = \pi r_{in}^2$). As can be seen, the force produced by the gas in the chamber mainly depends on the MFs sealing capacity. As shown in Fig. 1b, displacement of the upper glass causes change of the drop shape as well as the magnetic field intensity at the MFs interfaces. The inner interface of fluid moves to the higher H_i, while the outer becomes the lower H_0 due to the squeezing and radial motion of the MFs. Thus, the smaller the height (h) between magnet surface and upper glass it is, the higher the gas supporting force it provides.

3. Experimental section

3.1. Materials

In this paper, N35 NdFeB annular magnets magnetized in the axial direction were used with the size of Φ16 mm × Φ12 mm × 6 mm. To achieve different surface magnetic intensities, the magnets were heated in vacuum oven for different times. The final surface magnetic flux densities of the magnets were 91 mT, 195 mT, 250 mT and 270 mT, respectively.

Commercial MFs consisting of Fe_3O_4 nanoparticles dispersed in synthetic hydrocarbon carrier was chosen. It has a saturation magnetization (M_s) of 23.8 kA/m with the particle volume fraction of about 6.3%.

3.2. Supporting force tests

The supporting force tests were carried out using a stress testing platform, as shown in Fig. 2. The upper indenter is rigidly fixed with a force sensor. The moving velocity of the indenter in the axial direction is controlled at 0.01 mm/s by a reducer. The measuring range and resolution of the force sensor are 5 N and 0.001 N, respectively. Before each test, the sensor was clean and reset. For each magnet, the usage of MFs volume is 0.5 mL. The curve of the supporting force over the axial movement can be recorded by a data acquisition system. The maximum supporting force is defined when the gap between the indenter and magnet is 0.01 mm.

The experiments were divided into two groups: (1) single annular magnet with different surface magnetic flux densities; (2) four magnets with different distributions. Fig. 1a presents the image of one magnet covered with MFs and Fig. 3 shows the four magnets samples embedded in aluminium plate in square array. As can be seen in Fig. 3a, when the center space of the magnets is 25 mm, each magnet can be considered as an individual. It is interesting that one more enclosed chamber in the center of the magnets is formed when the four magnets connect together as shown in Fig. 3b.

3.3. Friction tests

Friction tests were carried out using a reciprocating sliding

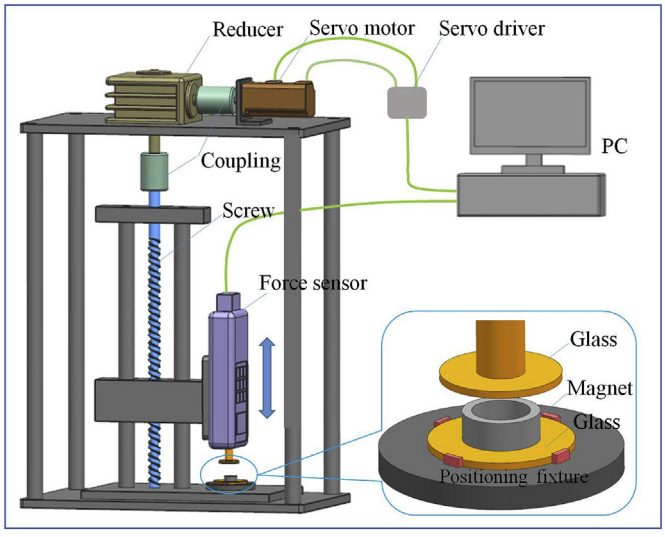

Fig. 2. The sketch map of the supporting force test system.

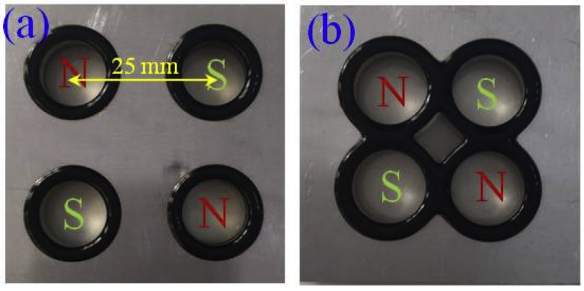

Fig. 3. Four magnets arrays with different gaps.

tribometer (Sinto Scientific, JAP). It consists of a stationary holder where a flat glass was placed and a reciprocating table where the magnet sample covered with MFs was mounted. To avoid the hydrodynamic effect, low speed of 0.1 mm/s was chosen. To further verify the supporting capacity, the normal load was chosen according to the supporting test results. Friction coefficient curve was auto collected and recorded using a personal computer controlled data acquisition system.

4. Results and discussion

Fig. 4 shows the supporting forces (F) plotted as function of the height (h). As can be see, all the forces increase when the upper indenter approaches to the magnet surface. For the magnet bottom unsealed sample, the load carrying capacity (F) only derives from the magnetostatic force of MFs (F_1). For MFs, each particle is a thermal activated nano-sized magnet in the carrier fluid. Under magnetic field, the magnetic moment of each particle will swerve in the direction of the external field, resulting in a macroscopic magnetization. The formation mechanism of the magnetostatic force involves in the transformation of the forces on individual particles to the bulk liquid. Theoretically, the achieved force is directly in proportion to the product of magnetization of the used MFs and the gradient of the applied magnetic field [14]. With the decreasing of the height, the gradient of field strength as well as the magnetic field imposed on MFs increases. Therefore, the force exerted on the individual permanent magnetic dipoles of the ferrite particles enhances, leading to the promotion of the magnetostatic force. According to the test results, the maximum magnetostatic force of MFs for static supporting is about 0.5 N/cm^2, taking account of the surface area of the annular magnet.

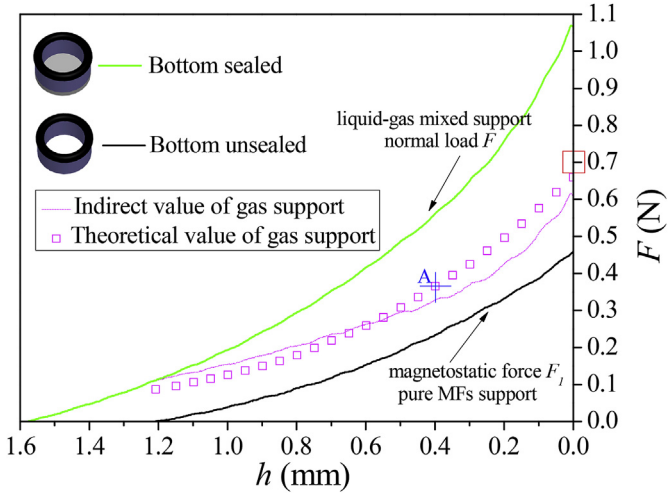

Fig. 4. The supporting forces plotted as function of the height. The solid line is experimental values, the dot is indirect value of the gas support, which is the difference between bottom sealed and unsealed value at the same height; the square is the theoretical value calculated according to Eq. (5).

As the bottom of the magnet sealed, the bearing capacity originates from the combined contributions of liquid (F_1) and gas support (F_2) together. Obvious improvement of the total force (F) was observed compared with pure MFs supporting (F_1) (see in Fig. 4). To gain more insight into the gas support, at the corresponding height, the magnetostatic force (F_1) is subtracted from the total force (F). Ignoring the effect of gas pressure on the MFs configuration, the difference ($F - F_1$) could approximately be regarded as the gas supporting force (F_2) (named indirect value of gas support in Fig. 4). As can be seen, the supporting force of gas increases gradually with the decreasing height (see in Fig. 4, dot line).

For comparison, the gas bearing was also calculated according to Eq. (5) and the description of the analytical model for computation was given in Fig. 1b. Moving down the upper glass in the vertical direction will cause the deformation of the MFs ring. When the up indenter is at a certain height, the location of the inner and outer interfaces of MFs in the gap depends on the magnetic field distribution.

Based on Eq. (5), the main task is to obtain the value of ($H_i - H_0$), since the values of M_s, μ_0 and A_F are the constants. Here, the solution of the problem is done numerically using magnetic field finite element method (FEM) by Ansoft Maxwell ver. 10.0 software. The geometrical and magnetic parameters input are based on the magnet. As mentioned before, the N35 NdFeB magnet with the size of Φ16 mm × Φ12 mm × 6 mm was used. The magnetic parameters can be set as follow: coercivity of H_c is −880 kA/m, remanence of B_r is 1.18 T and relative permeability of μ_r is 1.1. Thus, the magnetic field distributions at different height as a function of the radius can be achieved. After that, the theoretical value of the force (F_2) generated by the gas can be calculated. For an instant, when the dosage of MFs is 0.5 mL and the height (h) is fixed at 0.4 mm, the computed value of H_i is 2.85×10^5 A/m and H_0 is about 1.77×10^5 A/m. The vacuum magnetic permeability μ_0 is $4\pi \times 10^{-7}$ N/A^2 and the area ($A_F = \pi r_{in}^2$) is 1.13×10^{-4} m^2. The M_s of the MFs is about 2.38×10^4 A/m. Thus, the calculated force (F_2) is about 0.366 N and the value (point A in Fig. 4) is close to the indirect value of gas supporting. As can be seen in Fig. 4, the data of numerical calculation presents a similar variation trend as the indirect value of gas support.

Fig. 5 shows the effect of the surface magnetic flux density on the supporting forces (F). The magnets used are in the same geometry. As can be seen, the three forces increase with the decreasing of the height, presenting a similar tendency. The force values differ very much, and the magnet with higher magnetic flux density presents the higher force in general. Moreover, when the height (h) is smaller, the force difference becomes more significant. As mentioned above, the tested force is composed of the magnetostatic force (F_1) and sealed gas supporting

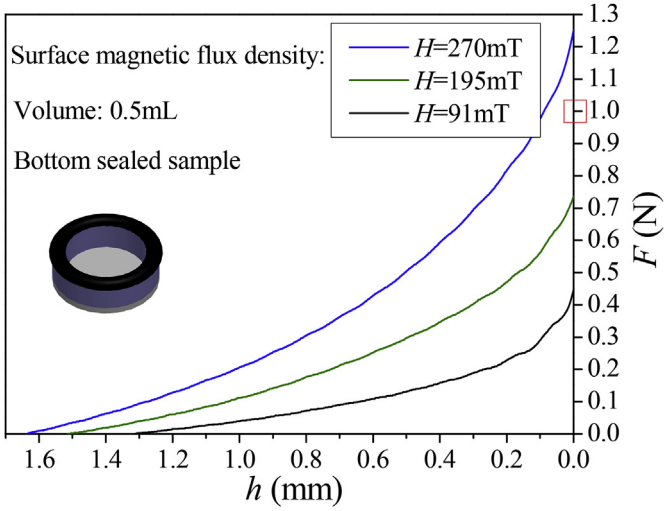

Fig. 5. Effects of surface magnetic flux density (H) on the supporting force (F).

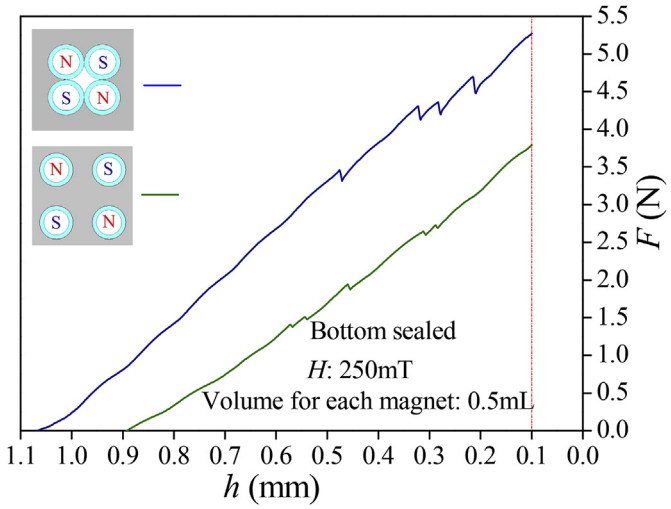

Fig. 6. Effect of magnet distribution on the supporting forces.

(F_2). On one hand, as the upper glass approaches to the magnet, the magnetostatic force (F_1) enhances due to the strengthened interaction of the magnetic particles subjected to the magnetic field. On the other hand, there is a fast growing of the magnetic field gradient crossing the MFs interfaces ($H_i - H_0$). Thus, the forces vary a lot especially at the small height position.

Fig. 6 presents the effect of magnet distribution on the supporting force. Naturally, the two samples both show higher forces compared with single magnet samples. Limited by the measuring range of the force transducer, each test had to be stopped at the height of 0.1 mm. For the magnets arranged with center space of 25 mm (see in Fig. 3a), each magnet can be considered as an individual and the four independent supporting units are formed. At the height of 0.1 mm, the force is about 3.76 N, which is almost 4 times of single magnet (0.9 N, see in Fig. 4). It is interesting that the sample in Fig. 3b presents much higher supporting force. Although the two samples are both composed of the same magnets, different supporting capacities appear. The possible reason should come from the magnet distributions.

To figure out the issue, the surface magnetic flux densities of the two samples were calculated using an Ansoft Maxwell 3D model. The magnetic flux densities are satisfied with the infinite far field boundary condition. The length of 1 mm of the magnet was divided into the maximum number of element 1000. For aluminium substrate, the maximum length of 13 mm was separated into the maximum number of element 1000. For surround region, the length of elements is 26 mm and the maximum number of element is 1000. During the calculating process, the value of error is set as 0.01%, which can meet a basic guarantee of the simulation accuracy.

As shown in Fig. 7a, the surface magnetic flux density is weak overall, and it mainly focused on the surface of each magnet. Obvious difference is observed in Fig. 7b. Due to the absorbing of the magnetic poles, magnetic field interactions play the dominate reason and the stronger magnetic intensity appears at the magnet contact boundary. More importantly, the contact boundaries form one more sealed space in the center of the sample. On one hand, the new formed chamber produces an extra gas supporting. On the other hand, since the magnetic flux density at the contact boundary is higher, it may generate larger pressure difference across the fluids interface compared with that of the single magnet chamber. That's the reasons why the magnet connecting sample (Fig. 3b) shows the larger force. The result suggests that proper magnet distribution is a practical path to enhance the bearing capacity.

The final aim of this study is to realize the full film lubrication based on the supporting force. In addition, the force is independent on the relative speed or the use of a pump. Thus, friction tests were carried out at special normal loads, which are chosen according to the supporting tests.

Fig. 8 shows the friction curves of single magnet supporting system at low sliding speed. In Fig. 8a, the normal load is fixed at 0.7 N, and the value is between the supporting forces of the bottom unsealed and sealed conditions (see Fig. 4). Compared with the dry friction, the coefficients decrease when lubricated with MFs. For the bottom unsealed one, the normal load is higher than its limit bearing capacity (0.45 N, see in Fig. 4). It means the tribo-pairs can not be totally separated by the supporting force. The normal load is partly carried by lubricant film and partly by asperity contact of the rubbing surfaces. The stable friction coefficient is about 0.05, which is in the mixed lubrication regime. This regime is in between the full film hydrodynamic and boundary. The total friction consists of hydrodynamic friction due to MFs shearing and boundary film friction at asperity contact locations.

However, for the bottom sealed sample, the maximum supporting force (1.05 N, see in Fig. 4) is higher than the value of normal load, similar to a hydrostatic lubrication. Meanwhile, according to Fig. 4, it can be estimated that the gap between the tribo-pairs is about 0.3 mm at the load of 0.7 N. Thus, tribo-pairs are totally separated from each other by the MFs and the enclosed gas. Friction force only comes from the shear of the MFs viscous, and the value of the coefficient is close to zero.

Friction tests were also conducted using the magnets with different surface magnetic field intensities. The load value of 1.0 N was used according to the supporting test results (see in Fig. 5). As can be seen in Fig. 8b, similar results were found.

When the weight of the object is lower than the generated force, then it may float on such supporting construction, so that the tribo-technical system has a friction force of zero. Most importantly, the load-carrying capacity of this construction does not depend on velocity and the force still exists between two plane parallels that are much different from hydrodynamic lubrication.

5. Conclusions

In this paper, the gas supporting force generated by MFs sealing is introduced. Theory analysis shows that the load carrying capacity of the

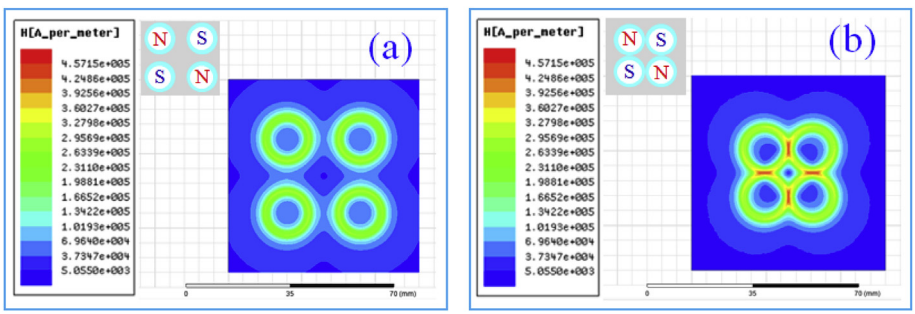

Fig. 7. The surface magnetic flux density with different magnet distributions.

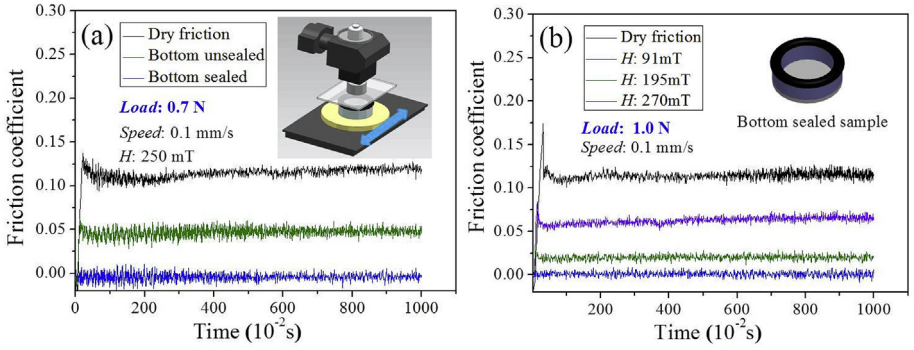

Fig. 8. Friction curves of the MFs supporting system.

gas bearing mainly lies on the MFs sealing capacity. The total force of the MFs bearing improves a lot as the sealed gas joins in. The influences of surface magnetic strength of magnet as well as magnet distribution on the supporting force were studies experimentally. The result shows that by increasing the magnet's surface magnetic strength, the load carrying capacity of the MFs bearing increases. Besides, proper magnet distribution is an efficient method to promote the bearing force. In addition, the total bearing capacity of such construction is also limited by the sizes and magnetic properties of the magnets.

For the hydrodynamic lubrication, the load-carrying capacity must rely on the relative speed of two surfaces. While based on such MFs sealed structure, the carrying capacity is produced by the mixed liquid-gas support. The most important thing is that such supporting force is independent from speed and the two frictional surfaces can be completely separated even at static condition. Therefore, ultralow friction coefficients can be achieved even at very low sliding speed. Such design pattern would be significant for solving the “cold welding” as well as the “stick-slip” phenomenon at low speed conditions, especially in precise sliding machine.

Acknowledgements

The authors are grateful for the support provided by the National Natural Science Foundation of China (No.51875278) and the Fundamental Research Funds for the Central Universities (No. NE2017104).

References

[1] Charles SW. The preparation of magnetic fluids. Lect Notes Phys 2003;594:3–18.
[2] Odenbach S. Ferrofluids—magnetically controlled suspensions. Colloid Surface Physicochem Eng Aspect 2003;217:171–8.
[3] Kanno T, Kouda Y, Takeishi Y, Minagawa T, Yamamoto Y. Preparation of magnetic fluid having active-gas resistance and ultra-low vapor pressure for magnetic fluid vacuum seals. Tribol Int 1997;30:701–5.
[4] Umehara N, Komanduri R. Magnetic fluid grinding of HIP-Si3N4 rollers. Wear 1996;192:85–93.
[5] Nakatsuka K. Trends of magnetic fluid applications in Japan. J Magn Magn Mater 1993;122:387–94.
[6] Huang W, Wang X. Ferrofluids lubrication: a status report. Lubric Sci 2016;28:3–26.
[7] Prajapati BL. Magnetic-fluid-based porous squeeze films. J Magn Magn Mater 1995;149:97–100.
[8] Oldenburg CM, Borglin SE, Moridis GJ. Numerical simulation of ferrofluid flow for subsurface environmental engineering applications. Transport Porous Media 2000;38:319–44.
[9] Huang W, Shen C, Wang X. Study on static supporting capacity and tribological performance of ferrofluids. Tribol Trans 2009;52:717–23.
[10] Bashtovoi VG, Bossis G, Kabachnikov DN, Krakov MS, Volkova O. Modelling of magnetic fluid support. J Magn Magn Mater 2002;252:315–7.
[11] Lampaert SGE, Spronck JW, RAJv Ostayen. Load & stiffness of a planar ferrofluid pocket bearing. The 17th nordic symposium on tribology. 2016.
[12] Wang Z, Hu Z, Huang W, Wang X. Elastic support of magnetic fluids bearing. J Phys Appl Phys 2017;50:435004.
[13] Li D, Xu H, He X, Lan H. Study on the magnetic fluid sealing for dry Roots pump. J Magn Magn Mater 2005;289:419–22.
[14] Rosensweig RE. Ferrohydrodynamics. Cambridge: Cambridge University Press; 1985.